Steel and Composite Structures, *Vol. 23, No. 2 (2017) 195-204*
DOI: https://doi.org/10.12989/scs.2017.23.2.195

Shake-table study of plaster effects on the behavior of masonry-infilled steel frames

Goran Baloevic *, Jure Radnic, Nikola Grgic and Domagoj Matesan

Faculty of Civil Engineering, Architecture and Geodesy, University of Split, Matice hrvatske 15, 21000 Split, Republic of Croatia

(*Received October 14, 2016, Revised December 02, 2016, Accepted December 19, 2016*)

Abstract. The effects of plaster on the behavior of single-story single-bay masonry-infilled steel frames under in-plane base accelerations have been experimentally investigated by a shake-table. Tested structures were made in a 1/3 scale, with realistic material properties and construction methods. Steel frames with high and low flexural rigidity of beams and columns were considered. Each type of frame was tested with three variants of masonry: (i) non-plastered masonry; (ii) masonry infill with conventional plaster on both sides; and (iii) masonry infill with a polyvinyl chloride (PVC) net reinforced plaster on both sides. Masonry bricks were made of lightweight cellular concrete. Each frame was firstly successively exposed to horizontal base accelerations of an artificial accelerogram, and afterwards, to horizontal base accelerations of a real earthquake. Characteristic displacements, strains and cracks in the masonry were established for each applied excitation. It has been concluded that plaster strengthens the infill and prevents damages in it, which results in more favorable behavior and increased bearing capacity of plastered masonry-infilled frames compared to non-plastered masonry-infilled frames. The load-bearing contribution of the adopted PVC net in the plaster was not noticeable for the tested specimens, probably due to relative small cross section area of fibers in the net. Behavior of masonry-infilled steel frames significantly depends on frame stiffness. Strong frames have smaller displacements than weak frames, which reduces deformations and damages of an infill.

Keywords: masonry-infilled frame; plaster; fiber-reinforcement; shake-table; earthquake

1. Introduction

Many buildings have visible plastered masonry walls. Herein, different types and thicknesses of plaster are used. The plaster strengthens the masonry and increases its bearing capacity under vertical and especially horizontal loads. That contribution is greater with better quality and thicker layer of a plaster. A relative contribution of plaster to the overall bearing capacity of masonry can be significant for thin masonry walls of poor quality. Reinforcing the plaster achieves further improvements in quality and the bearing capacity of masonry walls. Al-Chaar and Hasan (2002) performed both pseudo-static and shake table tests of unreinforced masonry walls retrofitted with fiberglass composite material applied as an overlay to only one side of the walls. Bairrão and Falcão Silva (2009) performed shaking table tests of two different reinforcement techniques using polymeric grids and a fiber-added mortar on an asymmetric limestone full-scaled structure. Juhásová *et al*. (2008) performed seismic tests of a masonry model reinforced on parts of a wall surface by vertical polymer grids bonded with fiber-reinforced plaster. Başaran *et al*. (2014) investigated the behavior of a single-story single-span masonry buildings subjected to seismic load on the shaking table, with a particular focus on the modification of structural response due to application of the polypropylene and steel reinforced plaster. De Santis *et al*. (2016) proposed and investigated steel reinforced grout strengthening system through shake table tests on a natural scale wall assemblage. The system comprises horizontal strips of ultra-high strength steel cords, externally bonded to the masonry with hydraulic lime mortar, and connectors to transversal walls, applied within the thickness of the plaster layer.

Masonry-infilled concrete and steel frames are often used in practice. In these structures, a plaster also contributes to their overall stiffness and bearing capacity. A relative contribution of plaster to their bearing capacity depends on the stiffness of a non-plastered frame, as well as on the frame-infill stiffness ratio. Žarnić (1994) tested one-bay, one-story, masonry infilled reinforced concrete frame specimens exposed to cyclic horizontal displacements. The intention was to analyze repair and strengthening technique by combining epoxy grouting and the application of reinforced cement plaster to both surfaces of the infill. Benedetti *et al*. (1998) performed shaking table tests of 24 half-scale two-story masonry buildings to study the seismic behavior and effectiveness of various retrofit techniques for masonry buildings. One of these techniques involved steel nets placed at each story level all around the building and covered with a shallow cement layer, thus originating a reinforced concrete band at those locations. Santhi *et al*. (2005) tested two single-bay, three-story space frames, one with brick masonry infill at upper floors and the other without infill. The frames were tested to failure, and the damaged soft-story frame was retrofitted with concrete

*Corresponding author, Ph.D.,
E-mail: goran.baloevic@gradst.hr

ISSN: 1229-9367 (Print), 1598-6233 (Online)

jacketing and subjected to same earthquake motions as the original frames. Shing *et al*. (2013) investigated the influence of retrofitting unreinforced masonry infill walls with engineered cementitious composite materials. In this study, shake-table tests were conducted on a three-story, two-bay, masonry infilled RC frame repaired by injecting epoxy into cracked mortar joints and strengthened with a glass-fiber reinforced polymer overlay (Koutromanos *et al*. 2013). Stempniewski *et al*. (2014) studied the effectiveness of a proposed retrofit scheme by attaching glass fiber textile on the brittle brick partition walls in the buildings using polyurethane glue and connecting them with the peripheral structural frames. Emami and Mohammadi (2016) tested five half-scaled single-story, single-bay steel frame specimens under cyclic lateral loading. Their study showed that the vertical load changes the cracking patterns and failure modes of the infill panels.

In this paper, the effect of plaster on the behavior of one-story masonry-infilled steel frames under in-plane horizontal base accelerations have been experimentally investigated by a shake-table. Tested structures were made in a reduced scale (1:3), with realistic material properties and construction methods. Two types of steel frames were considered: one with high and other with low flexural rigidity of beams and columns. Each type of a frame was tested with three variants of the infill: (i) non-plastered masonry infill; (ii) masonry infill with conventional plaster on both sides; and (iii) masonry infill with a polyvinyl chloride (PVC) net reinforced plaster on both sides. Masonry bricks made of lightweight concrete were used. Each frame was firstly exposed to horizontal base accelerations of an artificial accelerogram. Herein, the maximal amplitude of acceleration was successively increased from 0.1 g to 0.8 g. After that, the frames were exposed to horizontal base accelerations of a real earthquake. The maximal acceleration amplitude was increased from 0.1 g to 0.45 g, i.e., until failure of the frame. Characteristic displacements of the frame, strains in steel and masonry, as well as states of cracking in masonry were established for each applied base excitation. The main conclusions of the research are presented at the end.

2. Experimental research program

2.1 Basic data

The basic data regarding the tested one-bay, one-story masonry-infilled steel frames is shown in Fig. 1. The tested specimens represent a 1:3 scale model of the real structure, with real materials and construction methods. Steel frames with high and low flexural rigidity were considered separately, i.e., a so-called strong frame (SF) and a so-called weak frame (WF) were considered. A great difference in stiffness of the frames was adopted so their behavior could differ significantly under earthquake. Masonry brick elements made of cellular lightweight concrete with density of 450 kg/m^3 were used. Brickwork was performed by using prefabricated thin joint mortar. Each type of frame had three variants of masonry infill: (i) non-plastered masonry infill (SF-1, WF-1); (ii) masonry infill with pre-mixed plaster on

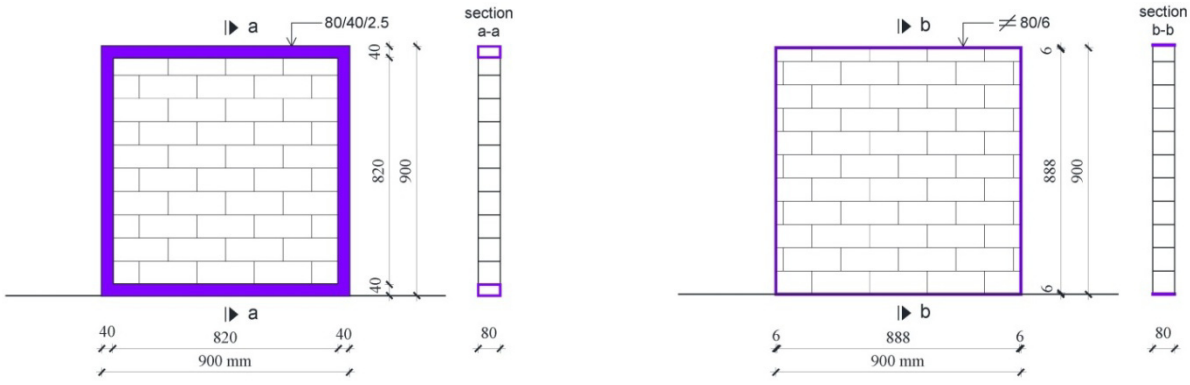

(a) Strong frame (SF) (b) Weak frame (WF)

Fig. 1 Basic geometry data of tested masonry-infilled steel frames

(a) Front view (b) Side view

Fig. 2 Tested structure on the shake-table

both sides (SF-2, WF-2); and (iii) masonry infill with pre-mixed plaster on both sides reinforced with a PVC net (SF-3, WF-3). Specimens were plastered with pre-mixed mineral fiber-reinforced plaster with a thickness of 10 mm on both sides. Extruded PVC net with quadrangular mesh for cracking-prevention of a plaster was used. The mesh size of the PVC net is 3.6 × 3.6 mm, having a unit weight of 160 g/m^2. The number of warp and weft threads per 100 mm of the net are 24 × 2 and 21, respectively. The net was embedded in the middle of the plaster layer. An additional mass of 3 tons was placed at the top of the frames, made of a concrete block 1 × 1 × 1.2 m, which simulated the mass of the supported floor. The block was fixed to the top of the frames. Frames were laterally constrained to prevent lateral buckling of columns.

Appropriate conclusions in terms of behavior and safety of a real structure can sometimes be hard to develop using results from tests on its smaller scaled model with actual material characteristics and under actual base acceleration. The oscillation period of the scaled model is k times lower than of the real structure, where k is a scale factor, and local material effects may differ significantly for the real structure and its scaled model. Since tests in this paper are conducted on the same model in order to investigate a relative influence of several parameters, it is believed that conclusions obtained on the scaled model are representative for the real structure as well.

2.2 Material properties

Strong steel frames were made of rectangular hollow section 80 × 40 × 2.5 mm tubes, while weak steel frames were made of 80 × 6 mm strips. All joints were welded. The frames were constrained at the base. The adopted steel was S235, with declared initial modulus of elasticity of 200 GPa. Brick elements have a declared compressive strength of 3 MPa. The tested uniaxial compressive strength of masonry was 2.18 MPa, the tensile strength by flexural test was 0.2 MPa, and the initial modulus of elasticity was 1.02 GPa. The tested uniaxial compressive strength of unreinforced plaster was 3 MPa, tensile strength 1 MPa and initial modulus of elasticity 3.5 GPa. The tensile strength, break elongation and elasticity modulus in the warp direction of the net were measured as 42.84 N/mm, 3.48% and 1.23 kN/mm, respectively. The tensile strength, break elongation and elasticity modulus in the weft direction of the net were measured as 48.68 N/mm, 3.94% and 1.24 kN/mm, respectively.

2.3 Instrumentation

Data acquisition from sensors during the shake-table experiments was ensured using the Hottinger Baldwin Messtechnik GmbH (HBM) QuantumX high-speed data acquisition system with 16 channels. The horizontal displacement of the top of a frame was measured by a type WA/100-L (HBM) inductive displacement transducer. The steel strains at the bottom of the columns were measured by glued strain gauges of type K-LY11-5/120 (HBM). The average masonry strains in the diagonal direction were measured by type WA/10-L inductive displacement transducers that were stretched over diagonal spans of masonry. To measure the acceleration of the top of a frame, a Kistler accelerometer of type 8640 with measuring range of ± 5 g and with automatic compensation of the gravitational acceleration was used. The sampling rate during the shake-table tests was 200 Hz. A video camera was used to monitor and record the structural deformations and crack patterns in the masonry.

2.4 Dynamic loading

A shake-table at the University of Split, in the laboratory for seismic testing at the Faculty of civil engineering, architecture and geodesy, was used to test the frames. The layout size of the shake-table is 4 × 4 m, and the maximal capacity is 20 tons. The shake-table can achieve a maximal displacement of ±150 mm, a maximal acceleration of up to 5 g, and frequencies from 0-20 Hz. The shake-table with a prepared specimen for testing is shown in Fig. 2.

The specimens were exposed to horizontal base accelerations of the shake table according to Fig. 3. Firstly, an artificial accelerogram was obtained with the computer software SIMQKE (Software SIMQKE 2016), as a superposition of sinus functions. The accelerogram was created from elastic design response spectrum according to Eurocode 8 (2011) for type 1 and soil type A (see Fig. 3(a)), with its modification for adequate simulation of very rigid structures such as the tested small scale specimens. A set of eight artificial accelerograms was generated by scaling the peak ground acceleration (PGA) for 0.1 g, i.e., PGA = n × 0.1 g; n = 1 – 8. After that, all frames were exposed to the set of five ground accelerations of the earthquake Petrovac, Montenegro (1979, orientation N-S). Herein, the original acceleration time history (see Fig. 3(b)) was scaled to have maximal acceleration amplitude PGA = n × 0.1 g (n = 1, 2, 3, 4 and 4.5). Tested specimens were first exposed to artificial accelerogram which is relevant for very rigid structures (see spectral acceleration in Fig. 3(a2)). After shaking and decrease of their stiffness, the specimens were further exposed to real accelerogram which is relevant for medium rigid structures (see spectral acceleration in Fig. 3(b2)).

3. Experimental results

Horizontal displacements and accelerations of the top of a frame, strains at the bottom of column, average masonry strains in diagonal directions, as well as crack states in masonry were observed for each applied base excitation. Measured variables are illustrated in Fig. 4. Only some obtained results are given hereafter. The results are shown for the artificial and the real accelerogram separately. Simultaneous results are given for the strong frame and for the weak frame, as well as for all three variants of the infill. In valorisation of graphically illustrated results of displacements and strains, it should be noted that in some cases permanent (irreversible) displacements and strains of frames remained due to previous applied excitations.

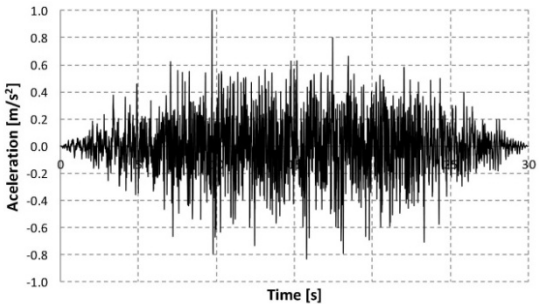

(a1) Acceleration time history

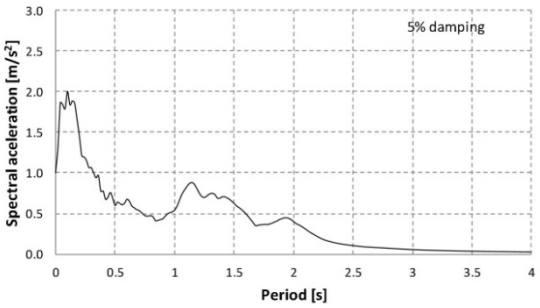

(a2) Elastic response spectra

(a) Artificial excitation

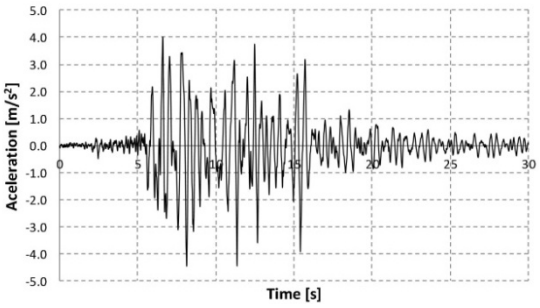

(b1) Acceleration time history

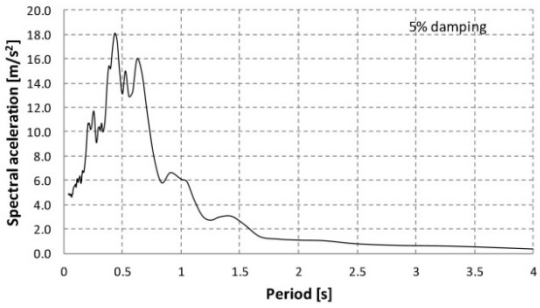

(b2) Elastic response spectra

(b) Earthquake Petrovac

Fig. 3 Acceleration time history and elastic response spectra of the applied ground motions

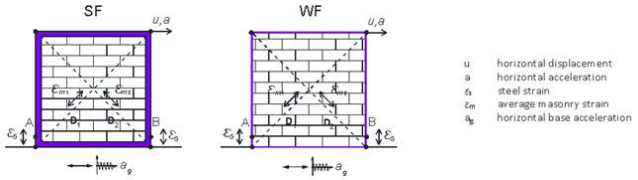

Fig. 4 Measured variables on the specimens

3.1 The effect of artificial accelerogram

As previously stated, the maximal amplitude of the acting artificial accelerograms was successively increased from 0.1 g to 0.8 g, with the increment of 0.1 g. Some measured results are shown in Figs. 5-10.

Horizontal displacements of the top of the frame in time are shown in Fig. 5. It can be noticed that the strong frame has far smaller displacements compared to the weak frame. The greatest displacement of the strong frame was about 2.6 mm, and for the weak frame about 5 mm. This results in a more favorable stress-strain state of infill for the strong frames than for the weak frames. In both variants of frame, the effect of infill types (infill stiffness) on displacement values was evident. The greatest displacements were for the non-plastered masonry-infilled frames. Frames with pre-mixed plaster and frames with a PVC net reinforced pre-mixed plaster had similar displacements. In all frames, a separation between the infill and columns and beams occurred already before the acting of the last artificial excitation. Inability of the infill to transfer tensile and shear stresses at the frame-infill interface caused the infill to behave like a strut in compression (in diagonal direction D1 and D2 interchangeably). By changing the motion direction, i.e., by alternation of tensile strut into compressive strut, an impact between column and infill occurred due to the incurred spacing between them during previous motion in opposite direction. This phenomenon was not so expressed for the strong frames, but was evident for the weak frames. During the acting of ground motion, the shape of deformed frames visually corresponded to a mirror rhomboid with changeable diagonals.

Steel strains at the bottom of the column at point A (on the left) are shown in Fig. 6. The strong frame had maximal compressive strain of about -0.55‰. Since the yielding strain of steel is about ±1.2‰, it is obvious that the steel strains in the stronger frames were elastic. The strains are similar for all types of infill, i.e., the stiffness of the infill in the strong frame had no significant influence on their value. The weak frame had far greater strains, up to -1.6‰. It indicates the appearance of nonlinearity in the column. The effect of infill stiffness is greater for the weak frames than for the strong frames. Herein, the greatest strains were for the frame with weakest infill (WF-1), and smallest for the frame with strongest infill (WF-3). Significant permanent strains remained in the column of frame WF-3, and especially of frame WF-2. In the weak frames, the effect of local bending of column due to its separation from the infill is probably present.

Steel strains at the bottom of the column at point B (on the right) are shown in Fig. 7. The strains are similar to those for the left column at point A. Frame WF-1 had far greater strains.

Average strains in the diagonal direction D1 and D2, conditionally called average masonry strains, are shown in

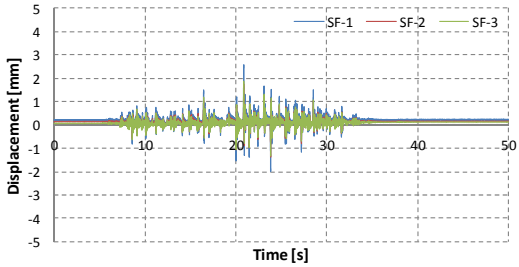

(a) Strong frame (SF)

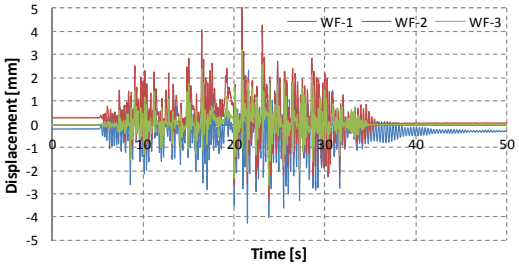

(b) Weak frame (WF)

Fig. 5 Horizontal displacements of the top of the frame for the artificial accelerogram with PGA = 0.8 g

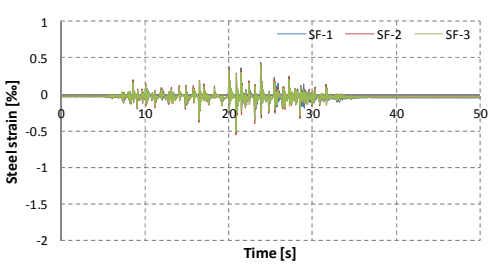

(a) Strong frame (SF)

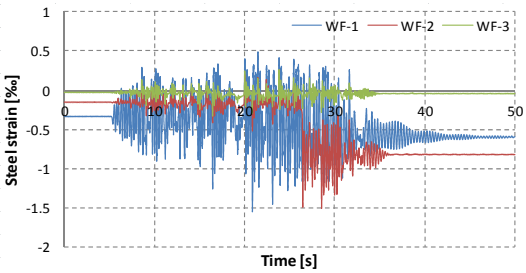

(b) Weak frame (WF)

Fig. 6 Steel strain (ε_s) at the point A at the bottom of column for the artificial accelerogram with PGA = 0.8 g

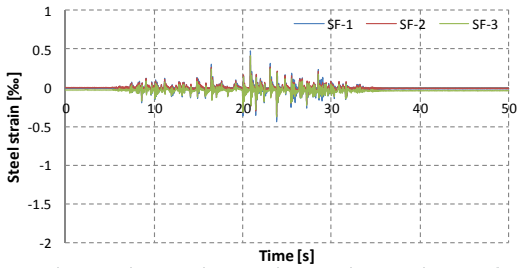

(a) Strong frame (SF)

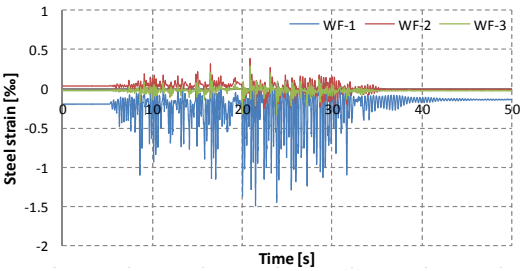

(b) Weak frame (WF)

Fig. 7 Steel strain (ε_s) at the point B at the bottom of column for the artificial accelerogram with PGA = 0.8 g

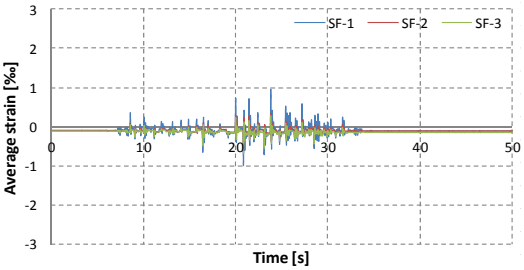

(a) Strong frame (SF)

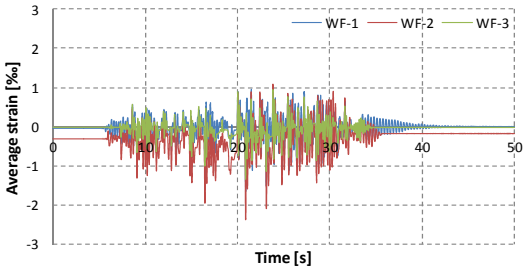

(b) Weak frame (WF)

Fig. 8 Average masonry strain (ε_{m1}) in diagonal direction D1 for the artificial accelerogram with PGA = 0.8 g

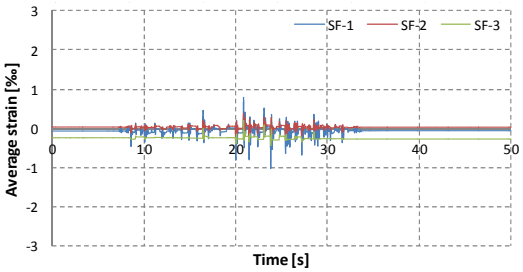

(a) Strong frame (SF)

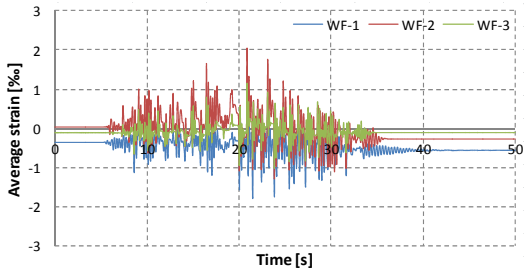

(b) Weak frame (WF)

Fig. 9 Average masonry strain (ε_{m2}) in diagonal direction D2 for the artificial accelerogram with PGA = 0.8 g

Figs. 8-9. The appearance of tension in the diagonal direction followed by separation of beam-column joint and infill should be taken into account in valorization of these results. Therefore, measured tensile strains also contain this spacing. Real tensile strains in masonry are significantly lower than strains shown in these figures. Except for the frames SF-1 and WF-1, cracks in masonry were not observed for this excitation, but only separation between frame and infill (almost at all interfaces). Great compressive strains in struts resulted in damage of the infill at corners, especially for the weak frames. It should be noted that masonry consisted of brick elements with low strength. The type of infill has small influence on the strain values in diagonal directions.

Horizontal accelerations of the top of the frames are shown in Fig. 10. Average values are slightly greater for the strong frames, if extremes of the weak frames are excluded. These extremes are the result of the impact between column and infill when the top of the frame changes the motion direction, i.e., when tensile strut becomes compressive strut.

Peak horizontal displacements of the top of frames for different maximal amplitudes of artificial accelerograms are shown in Fig. 11. It is noticeable that by increasing the PGA, displacements of the frames are also increased. The effect of frame stiffness is also noticeable, especially for the weak frames. Strong infill results in smaller displacements of the frame. However, the frames with plastered masonry have smaller displacements than the non-plastered masonry-infilled frames. The adopted PVC net in plasters had a very small influence on the displacements of the frames. Peak steel strains at the bottom of the column at point A for different maximal amplitudes of artificial accelerograms are shown in Fig. 12. By increasing the PGA, strains in the columns are also increased. This effect is the most evident for the weak frame WF-1 under excitations with greatest accelerations. By increasing the infill stiffness, strains in the columns of the weak frames are decreasing. This effect is negligible for the strong frames.

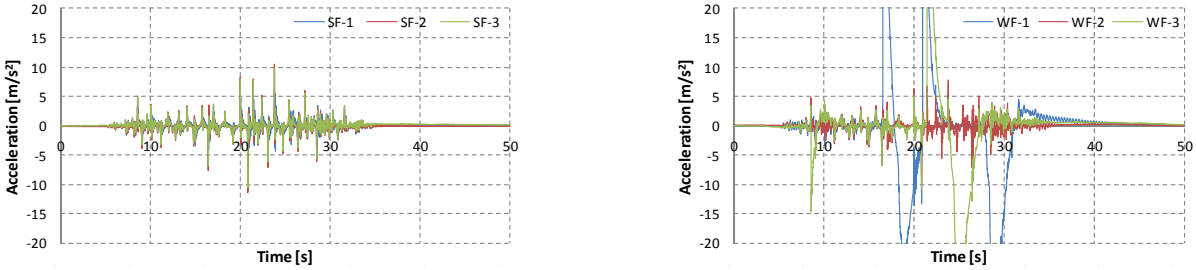

(a) Strong frame (SF) (b) Weak frame (WF)

Fig. 10 Horizontal accelerations of the top of the frame for the artificial accelerogram with PGA = 0.8 g

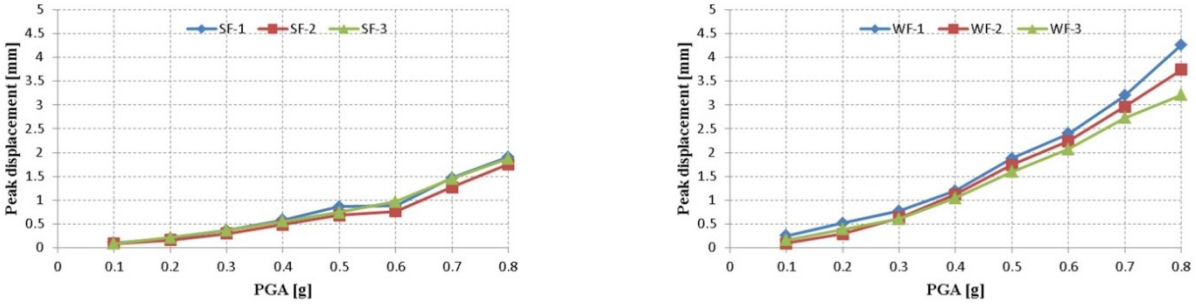

(a) Strong frame (SF) (b) Weak frame (WF)

Fig. 11 Peak horizontal displacements of the top of the frame for the artificial accelerograms

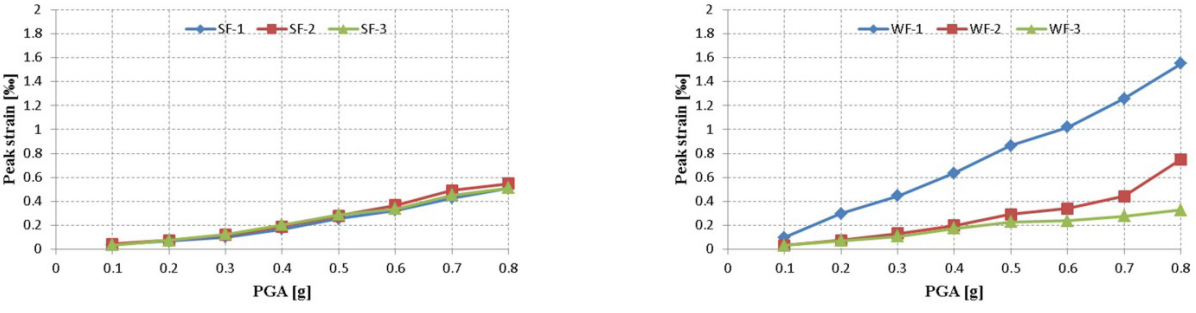

(a) Strong frame (SF) (b) Weak frame (WF)

Fig. 12 Peak steel strains (ε_s) at the point A at the bottom of column for the artificial accelerograms

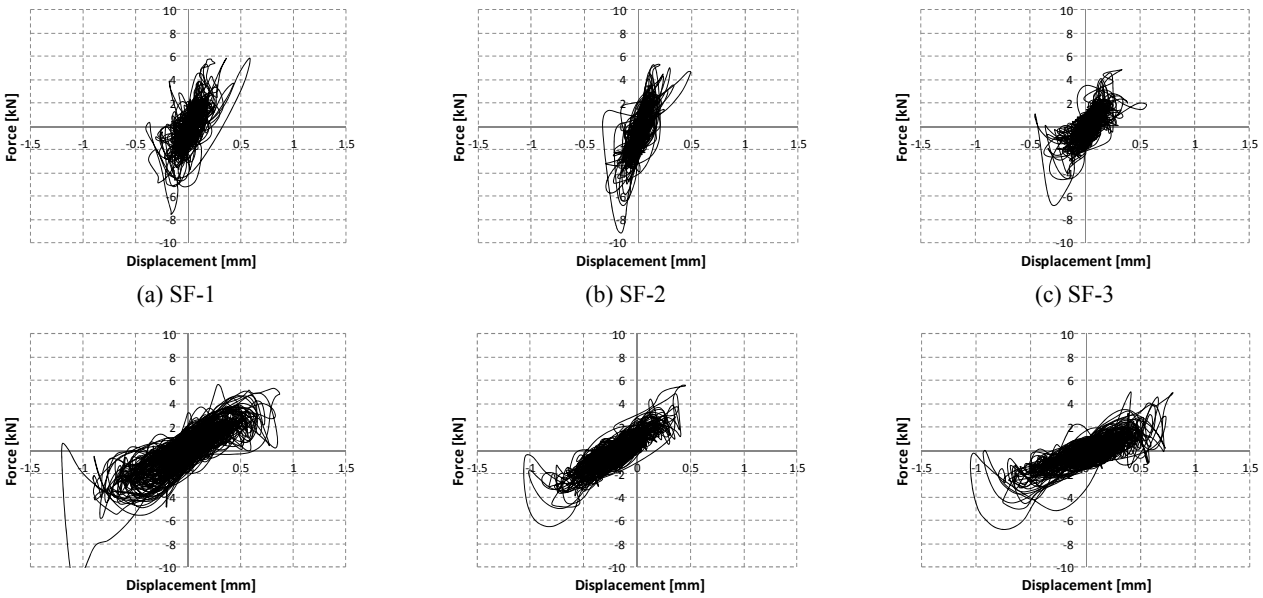

(a) SF-1 (b) SF-2 (c) SF-3

(d) WF-1 (e) WF-2 (f) WF = 3

Fig. 13 Shear force-displacement relationship for artificial accelerogram with PGA = 0.4 g

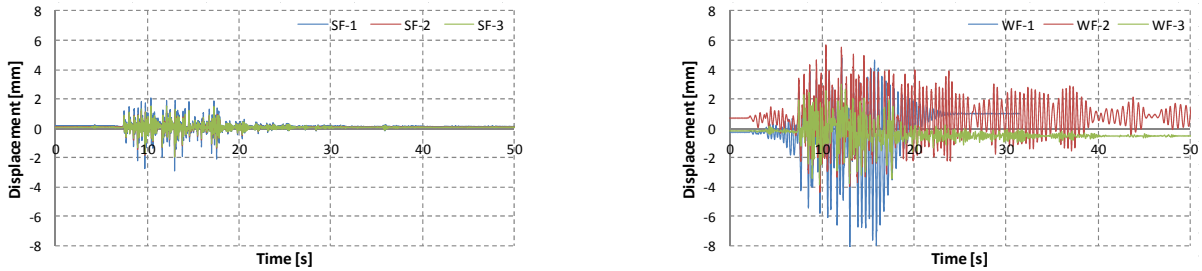

(a) Strong frame (SF) (b) Weak frame (WF)

Fig. 14 Horizontal displacements of the top of the frame for the earthquake Petrovac with PGA = 0.45 g

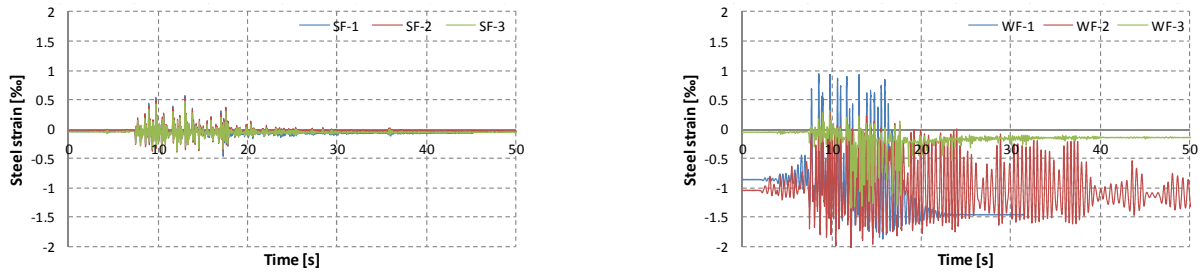

(a) Strong frame (SF) (b) Weak frame (WF)

Fig. 15 Steel strain (ε_s) at the point A at the bottom of column for the earthquake Petrovac with PGA = 0.45 g

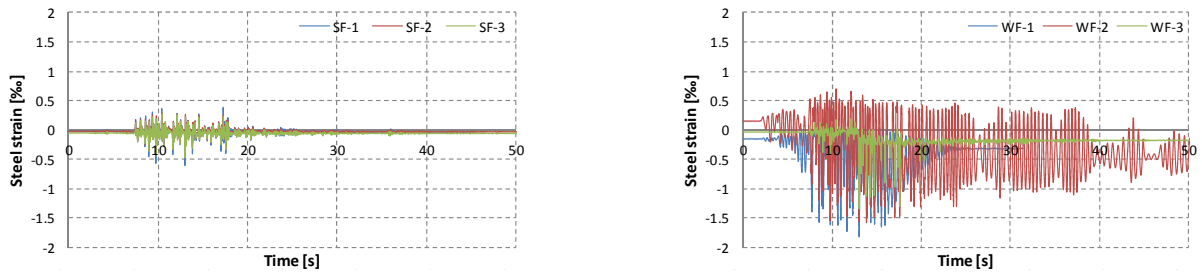

(a) Strong frame (SF) (b) Weak frame (WF)

Fig. 16 Steel strain (ε_s) at the point B at the bottom of column for the earthquake Petrovac with PGA = 0.45 g

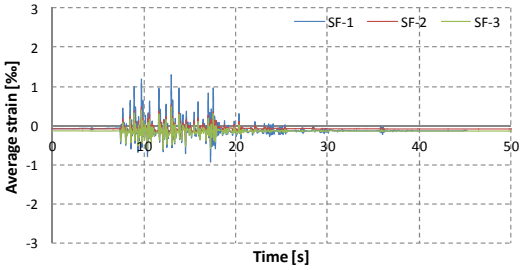

(a) Strong frame (SF)

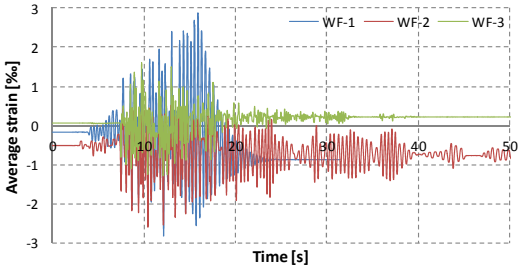

(b) Weak frame (WF)

Fig. 17 Average masonry strain (ε_{m1}) in diagonal direction D1 for the earthquake Petrovac with PGA = 0.45 g

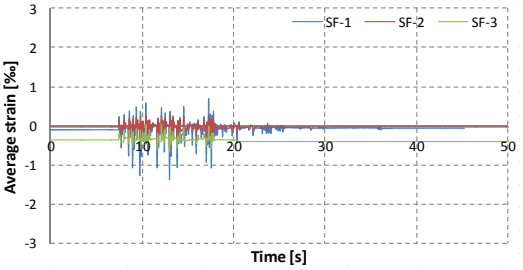

(a) Strong frame (SF)

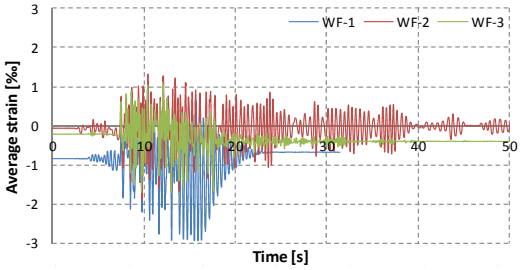

(b) Weak frame (WF)

Fig. 18 Average masonry strain (ε_{m2}) in diagonal direction D2 for the earthquake Petrovac with PGA = 0.45 g

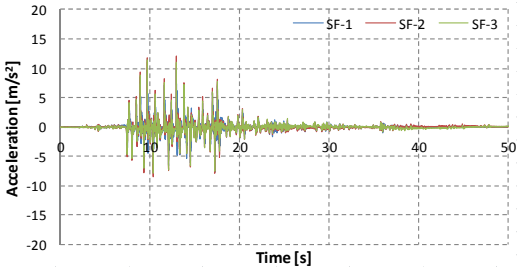

(a) Strong frame (SF)

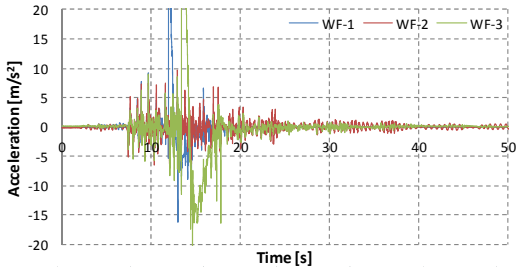

(b) Weak frame (WF)

Fig. 19 Horizontal accelerations of the top of the frame for the earthquake Petrovac with PGA = 0.45 g

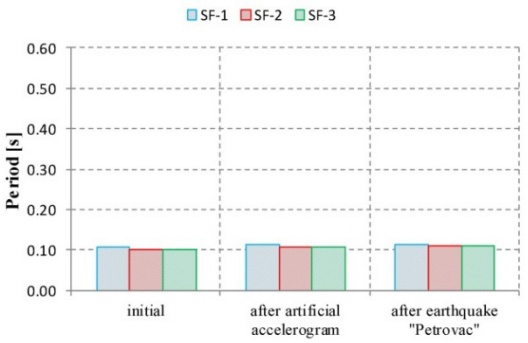

(a) Strong frame (SF)

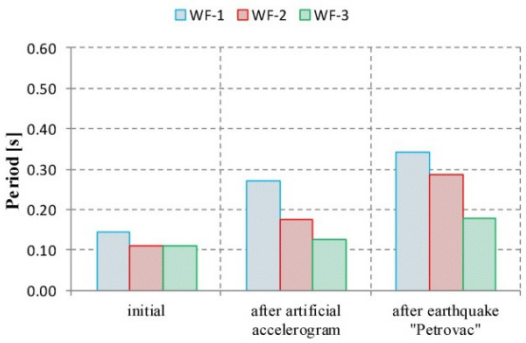

(b) Weak frame (WF)

Fig. 20 Natural periods of vibration for tested specimens

The shear force developed at the top of frames is evaluated from the measured horizontal acceleration and the associated mass of the concrete block. The shear force-displacement relationship for all specimens under artificial accelerogram with PGA = 0.4 g is shown in Fig. 13.

3.2 The effect of the real accelerogram

Like previously stated, after being exposed to successively increased accelerations of artificial ground motion, all frames were further exposed to successively

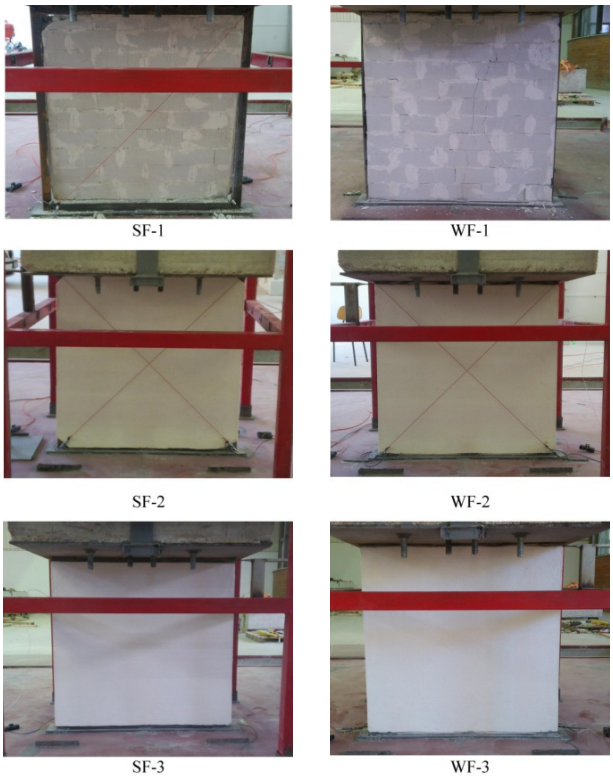

(a) Strong frame (SF) (b) Weak frame (WF)

Fig. 21 Final deformations and crack states of the infilled frames at the end of tests

increased accelerations of the earthquake Petrovac. Maximal acceleration amplitude in the applied excitations was PGA = 0.1 g, 0.2 g, 0.3 g, 0.4 g and 0.45 g. Only some results for accelerogram with PGA = 0.45 g are given in Figs. 13-18. Same variables are shown as for artificial ground motion in Figs. 5-10. By comparing measured values of corresponding variables, it can be concluded that results of the artificial accelerogram are compatible with results of the real accelerogram. It should be noted that tested frames were already previously damaged due to acting of the artificial accelerograms. In the interpretation of the results given in Figs. 14-19, it should be taken into account that large displacements and deformations of the specimen WF-1 occurred during the test, so the excitation was aborted at t = 15.8 s to prevent further collapse of the specimen.

The white noise wave was used to shake the specimens in order to monitor the change of their dynamic properties before the test and after each two sets of accelerations. The corresponding natural periods of vibration for all specimens are shown in Fig. 20. The change in stiffness at the end of all tests is more expressed for the weak frames than for the strong frames.

Final deformations and crack states of the infilled frames at the end of all tests are presented in Fig. 21. All plastered infilled frames (SF-2, SF-3, WF-2, WF-3) had no visible cracks in the masonry. Frame WF-1 had great cracks in the masonry, while frame SF-1 had small cracks in the masonry. Separation between the frame and the masonry occurred for all tested specimens, which was more evident for the weak frames. All frames had damages and crushing in the infill at the corners.

4. Conclusions

Conclusions below were formed based on the performed experimental research.

Behavior of masonry-infilled steel frames under earthquake loading significantly depends on the frame stiffness. Strong steel frames have smaller displacements than weak steel frames, which reduces deformations of the infill and prevents its damage. In relation to the weak frames, strong frames generate greater seismic (inertial) forces, but also have greater resistance. Weak frames have greater displacements than strong frames. This results in greater deformations of the infill, i.e., in its possible damage and larger separation (crack) at the infill-frame interface.

The stiffness of the masonry contributes to the overall stiffness of the infilled steel frames. Stronger infill increases inertial forces, but also has greater resistance than weaker infill. By testing the specimens, stronger infill showed more favorable behavior than weaker infill. However, in relation to the non-plastered masonry, masonry plastered on both sides ensured greater resistance and reduced deformability of the system and reduced cracks in the masonry.

Plastered infilled frames had no visible cracks in the infill. Separation between the frame and the infill occurred for all tested specimens. The separation was greater in the weak frames than in the strong frames. Crushing and damages of the infill in the corners occurred for all tested specimens, which was greater in the strong frames than in the weak frames.

The load-bearing contribution of the adopted PVC net in the plaster was not noticeable in the tested specimens, which is probably the consequence of the relatively small cross-section area of fibers in the net.

Investigations on behavior of infilled frames with plastered masonry under earthquake are in progress, with variants of different type, cross section area and elasticity modulus of a fiber net reinforcement in the plaster.

Acknowledgments

This work was supported by the funds of the Ministry of Science, Education and Sport of Croatia. The authors appreciate their financial support.

References

Al-Chaar, G.K. and Hasan, H.A. (2002), "Dynamic response and seismic testing of CMU walls rehabilitated with composite material applied to only one side", *Proceedings of the Institution of Civil Engineers - Structures and Buildings*, **152**(2), 135-146.

Bairrão, R. and Falcão Silva, M.J. (2009), "Shaking table tests of two different reinforcement techniques using polymeric grids on an asymmetric limestone full-scaled structure", *Eng. Struct.*, **31**(6), 1321-1330.

Başaran, H., Demir, A., Bagci, M. and Ercan, E. (2014), "Shaking table study of masonry buildings with reinforced plaster", *Gradjevinar*, **66**(7), 625-633.

Benedetti, D., Carydis, P. and Pezzoli, P. (1998), "Shaking table tests on 24 simple masonry buildings", *Earthq. Eng. Struct. Dyn.*, **27**(1), 67-90.

De Santis, S., Casadei, P., De Canio, G., de Felice, G., Malena, M., Mongelli, M. and Roselli, I. (2016), "Seismic performance of masonry walls retrofitted with steel reinforced grout", *Earthq. Eng. Struct. Dyn.*, **45**(2), 229-251.

Emami, S.M.M. and Mohammadi, M. (2016), "Influence of vertical load on in-plane behavior of masonry infilled steel frames", *Earthq. Struct., Int. J.*, **11**(4), 609-627.

HRN EN 1998-1:2011 (2011), Eurocode 8: Design of structures for earthquake resistance - Part 1: General rules, seismic actions and rules for buildings, European Committee for Standardization, (EN 1998-1:2004+AC:2009).

Juhásová, E., Sofronie, R. and Bairrão, R. (2008), "Stone masonry in historical buildings - Ways to increase their resistance and durability", *Eng. Struct.*, **30**(8), 2194-2205.

Koutromanos, I., Kyriakides, M., Stavridis, A., Billington, S. and Shing, P.B. (2013), "Shake-table tests of a 3-story masonry-infilled RC frame retrofitted with composite materials", *J. Struct. Eng.*, **139**(8), 1340-1351.

Santhi, M.H., Knight, G.M.S. and Muthumani, K. (2005), "Evaluation of seismic response of soft-storey infilled frames", *Comput. Concrete, Int. J.*, **2**(6), 423-437.

Shing, P.B., Koutromanos, I. and Stavridis, A. (2013), "Seismic performance of masonry-infilled RC frames with and without retrofit", *J. Earthq. Tsunami*, **7**(3), Article No. 1350023.

Software SIMQKE (2016), The Earthquake Engineering Online Archive, University of California, Berkley, CA, USA. http://nisee.berkeley.edu/elibrary/

Stempniewski, L., Mowrtage, W. and Urban, M. (2014), "Seismic collapse prevention of Non-Structural infill masonry using eq-top: an easy earthquake fibre retrofitting system", *Arab. J. Sci. Eng.*, **39**(3), 1599-1605.

Žarnić, R. (1994), "Experimental investigation of the R/C frame infilled by masonry wall," *Int. J. Eng. Model.*, **7**(1-2), 37-45.

CC